JOURNAL OF CATALYSIS 148, 100–112 (1994)

Cyclopropane Reactions over Brønsted, Cation, and Metal Sites in Ni/NaX Zeolites

Mark W. Simon,* C. O. Bennett,† and Steven L. Suib*,†,[1]

*U-60, Department of Chemistry and †Department of Chemical Engineering and Institute of Material Sciences, University of Connecticut Storrs, Connecticut 06269-3060

Received September 20, 1993; revised March 1, 1994

The reactions of cyclopropane in helium and hydrogen were investigated over two different loadings (10.7 and 6.0 wt%) of ion-exchanged Ni/NaX zeolites. The effects of reduction temperatures and hydrogen treatment times on catalytic activity and acidity were studied. Apparent activation energies ranged from 35.5 to 95.4 kJ/mol for isomerization reactions over two loadings of Ni/NaX zeolite reduced under different conditions. Rates of isomerization, hydrogenation, and hydrogenolysis are also reported. Deactivation and regeneration of catalysts are discussed. Particle sizes of 8.9 and 17.3 nm were observed in highly reduced Ni zeolites. Sintering of Ni was observed on the surfaces of the zeolite crystallites. Temperature programmed reduction studies show that stoichiometric amounts of H_2 were used to completely reduce all Ni in the samples. Infrared analysis of chemisorbed pyridine on these materials show that higher loadings of Ni result in higher initial acidities. Increased amounts of reduced Ni significantly increase the number of Brønsted sites on the surface of the catalyst. Electron paramagnetic resonance revealed that Ni^+ was present in low loaded Ni/NaX samples upon reduction at low temperatures (350°C), while higher reduction temperatures (450°C) resulted in a broad EPR signal corresponding to Ni^0 only. Na vapor deposition experiments, designed to selectively poison Brønsted sites on the catalyst, reveal that Ni^+ ions are active in cyclopropane isomerization reactions at high temperatures.

1. INTRODUCTION

Highly dispersed Ni particles have been known to be of great importance as hydrogenation and hydroisomerization catalysts (1). Transition metal cation-exchanged zeolite catalysts have been applied in the oxidation of hydrocarbons at a relatively low temperature. The active species in these catalysts were determined to be transition metal cations in the zeolite (2, 3). The multivalent cation-exchanged zeolites have solid acid properties, which have been often applied as useful catalysts in reactions which follow a pathway through a carbenium ion intermediate (4).

The skeletal isomerization of cyclopropane (c-C_3H_6) to propylene is a widely used test for the investigation of the activity of acid-type solid catalysts (5–8). The reaction of c-C_3H_6 with hydrogen has been studied by several researchers on metal supported catalysts (9–13).

Deuterium, kinetic, and mechanistic studies have shown that hydrogenation of c-C_3H_6 to propane through an intermediate of propylene was unlikely (14–16). In these investigations, propane was the only reaction product observed and there was no evidence for the formation of methane and ethane in hydrogenolysis reactions. This observation can be attributed to reaction conditions, the nature of the catalyst, and the interaction between the metal and the support. Taylor *et al.* discovered that the nature of the support has a marked effect on the catalytic properties of nickel, far greater than the effects of differences in dispersion of the metal on the support (17).

c-C_3H_6 isomerization reactions have been found to proceed readily over acidic catalysts at relatively low temperatures (15, 18, 19), while much higher temperatures were required for this same reaction on metals (20). Activation energies of 40–70 kJ/mol have been reported for c-C_3H_6 hydrogenation and hydrogenolysis reactions over Ni supported on SiO_2 (21).

On the basis of kinetic studies, mechanistic ideas of cyclopropane ring opening have been proposed. Ring opening is thought to occur upon sorption of c-C_3H_6 to the metal or acid sites (8, 14) or through the interaction between the active sites and delocalized pi electrons of cyclopropane, whose carbon atoms exhibit sp^2 hybridization (10). It is expected that c-C_3H_6 is less firmly bound to metal surfaces than hydrogen (9, 10, 14).

The steady state kinetic studies in this paper are one of very few in recent times on c-C_3H_6 reactions over Ni supported catalysts. Gas chromatography methods were used to monitor reaction products and obtain kinetic data for mechanistic ideas. Deactivation is monitored for isomerization, hydrogenation, and hydrogenolysis reactions.

[1] To whom correspondence should be addressed.

0021-9517/94 $6.00

This study uses zeolites as a support, unlike previous work on silica and alumina (12, 21). Modern techniques are available to characterize Ni supported on zeolites. Electron paramagnetic resonance, X-ray diffraction, Fourier transform infrared spectroscopy, temperature programmed reduction reactions, and atomic absorption techniques are used to characterize metallic and acidic sites in this mixed metal–acid catalytic system.

To our knowledge c-C_3H_6 isomerization reactions have not been applied to the Ni^{2+}/NaX zeolite system. We have chosen this system because TPD experiments with c-C_3H_6 in various diluent gases over Ni^{2+}/NaX have been previously studied (30). c-C_3H_6 was chosen as the reactant because earlier work in this area with Eu^{3+}/NaX showed that c-C_3H_6 was very effective in probing Brønsted acidity. Kinetic data and sodium poisoning studies are applied to reaction mechanisms and determining active species on the catalyst.

II. EXPERIMENTAL SECTION

A. Ion-Exchange of Zeolites

Solutions of $Ni(NO_3)_2 \cdot 6H_2O$ (obtained from Aldrich, Milwaukee, WI) were prepared to concentrations of 0.10 and 0.01 *M* in distilled deionized water (DDW). About 100 ml of each solution was used to ion-exchange 1 g of 60-mesh NaX zeolite (Linde 13 X, from Alfa Ventron, Danvers, MA). Ion-exchanges were done at room temperature in stirred round bottom flasks for 18 h followed by three washings of 5 ml of DDW. Samples were then filtered and dried in an oven at 110°C for 5 h.

B. Dehydration and Reduction Treatment of Catalysts

All Ni^{2+}/NaX zeolite samples were extensively dehydrated under vacuum prior to reduction and catalytic reactions. Samples were dehydrated on a vacuum line from room temperature to 400°C. A heating rate of 1°C/min and a vacuum of 5×10^{-6} Torr were used in this procedure. The dehydrated sample was sealed off, brought into a dry box, and loaded into the catalytic reactor. Previous high resolution mass spectrometry analyses on NaX and NaA zeolites dehydrated by this same method show no evidence of H_2O present upon heating to 400°C (30).

Dehydrated Ni^{2+}/NaX samples were reduced on line in the same reactor used for c-C_3H_6 isomerization and hydrogenation reactions. Reduction of Ni in H_2 was done for both Ni loadings of dehydrated NaX. Three different treatment procedures were followed. First, Ni^{2+}/NaX was reduced at 350°C for 4 h in H_2 at 30 cm^3/min, followed by cooling to room temperature in He. The second reduction treatment was at 450°C for 4 h under the same conditions. Finally, the same sample was heated to 450°C for 19 h under H_2 (30 cm^3/min). Steady-state catalytic experiments were run immediately after each treatment procedure, before proceeding with subsequent reductions. Sample labeling and description of reduction treatments are shown in Table 1.

C. Steady-State Catalysis

Experiments were run with completely dehydrated zeolites in a temperature range between 130 and 360°C. Temperatures were adjusted for the various loadings of Ni/NaX, particularly in the unreduced samples, in order to obtain conversions between 10 and 15% at the beginning of the reaction and 1 to 5% at steady state times. Five different temperatures were usually used in a 50 to 100°C range and at 10 to 20°C intervals. Flow rates were held constant at 30 ml/min for all reactions.

A 0.50% mixture of c-C_3H_6 in He was studied first for isomerization reactions, followed by a 0.50% mixture of c-C_3H_6 in H_2 for hydrogenation reactions. CP grade c-C_3H_6 (99.9% pure) was obtained from Matheson Gas Co., E. Rutherford, NJ. Helium and hydrogen (dehydration, diluent, and reduction gases) were zero grade obtained from Zero All-Gas, Co., Hartford, CT. Less than 10 ppm of propylene was measured by gas chromatography in the 0.5 mol% mixtures. No other hydrocarbon impurities were detected. Water and oxygen were also undetectable (using traps) in previous mass spectrometry analyses of 0.5% c-C_3H_6 (30). Propylene concentrations were corrected for propylene impurities in the c-C_3H_6 gas mixture. A Matheson catalytic gas purifier (Model 6406) was used to remove low levels of O_2 and H_2O from treatment gases and reaction mixtures.

Exactly 50 mg of pure sample (no diluent) was used to form a fixed-bed stainless steel reactor having a length of 30 cm and an inside diameter of 5 mm (22). Samples were supported on 100 mesh stainless steel screens and glass wool. The bed depth was less than 1 cm. A thermal conductivity detector (TCD) was used with a 5880 A Hewlett

TABLE 1

Catalyst Labeling According to Hydrogen Pretreatment and Ni Loading

Catalyst	Solution ion-exchange conc.	Time (h)	Temperature (°C)
A	0.10 *M*	No reduction	—
B	0.10 *M*	4	350
C	0.10 *M*	4	450
D	0.10 *M*	19	450
E	0.01 *M*	No reduction	—
F	0.01 *M*	4	350
G	0.01 *M*	4	450
H	0.01 *M*	19	450

Packard gas chromatograph (GC) for analysis. Samples were regenerated at 380°C in He (30 cm^3/min) to restore activity to original levels for isomerization reactions only. For hydrogenation reactions, complete restoration of the catalyst to original conversion levels in He was not obtainable. This will be addressed later in this paper. Detailed information on GC analyses, detector calibrations, reactor design, and the flow system with heat zones can be found elsewhere (18).

Data were analyzed for the steady-state experiments by using the material balance:

$$\text{Out} - \text{In} = \text{Rate} - \text{Accumulation}. \quad [1]$$

In our analyses, accumulation has a value of zero at steady-state. The simplified expression becomes,

$$\text{Rate} = \text{Out} - \text{In}. \quad [2]$$

For propylene isomerization, the rate of propylene production or cyclopropane disappearance is

$$\text{Rate} = (PQ_0/RT_0)y_{C_3H_6}/W, \quad [3]$$

where P is total pressure (1 atm), Q_0 is flow rate in cm^3/s (ambient), R is the ideal gas constant (82.057 cm^3–atm/mol K), W is the weight of the catalyst, $Y_{C_3H_6}$ is the mole fraction of C_3H_6 leaving the reactor, and T_0 is ambient temperature in K. Rate has units of mol s^{-1} g^{-1}.

For hydrogenolysis, the rate of cyclopropane disappearence is

$$\text{Rate} = (PQ_0/RT_0)(y_{CH_4}, y_{C_2H_6})/W, \quad [4]$$

where y_{CH_4} and $y_{C_2H_6}$ are the mole fractions of methane and ethane leaving the reactor.

For hydrogenation,

$$\text{Rate} = (PQ_0/RT_0)y_{C_3H_8}/W, \quad [5]$$

where $y_{C_3H_8}$ is the mole fraction of propane leaving the reactor.

In addition, apparent activation energies (E_a) for cyclopropane ring opening were obtained by plotting ln (Rate) vs $1/T$ $(K)^{-1}$ using the following relationships:

for isomerization,

$$\text{Rate} = kf(y_{c\text{-}C_3H_6}) \quad [6]$$

for hydrogenation and hydrogenolysis,

$$\text{Rate} = kf(y_{H_2}, y_{c\text{-}C_3H_6}). \quad [7]$$

Activation energies are expressed in kJ/mol.

D. Characterization

1. *Atomic absorption.* Exactly 70 mg of sample was dissolved in 10 ml of HF (conc), 10 ml HNO_3 (conc), and 5 ml HCl (conc). The samples were then digested in acid bombs by microwave heating. Following microwave digestion, the samples were brought to a total volume of 100 ml with DDW.

A Perkin-Elmer (PE) 5100 atomic absorption spectrometer equipped with a graphite furnace and an autosampling system (PE AS-60) was used in the analysis for Ni concentrations. A Zeeman background correction was taken. A PE HGA-600 temperature programmer was used to ensure accurate heating rates and temperatures.

2. *Temperature programmed reduction(TPR).* TPR studies were carried out on the 10.7 wt% Ni/NaX samples (A, B, C, and D). TPR experiments were performed on sample A in order to determine the amount of H_2 required for complete reduction of all Ni^{2+} present in the high loading of Ni/NaX. The extent of reduction in samples B, C, and D could then be determined by subtracting the hydrogen consumption of these samples from that of sample A, assuming that reduction of sample A was complete.

Exactly 30 mg of the 10.7% Ni/NaX zeolite was loaded in a quartz tube reactor and dehydrated *in situ* at 380°C under He for 8 h. A temperature program rate of 15°C/min was used to increase the temperature from reduction treatment temperatures to 670°C. A 4.0% H_2/Ar mixture was used for TPR studies. A thermal conductivity detector (TCD) was used to detect H_2 consumed. Ar carrier gas to the chromatograph was used to increase the sensitivity of the H_2 signal. Water formed during the reduction process was removed by anhydrous magnesium perchlorate.

3. *X-ray diffraction.* X-ray powder diffraction (XRD) experiments were done on a Scintag Model PDS 2000 diffractometer. Samples were mounted on glass slides by sprinkling powder on the slides to avoid preferential ordering. Full scans between 5° and 60° 2θ and step and multiple scans with peak averaging were carried out between a d-spacing of 2.073 and 1.952 Å. This d-spacing, which corresponds to the most intense of two peaks found in a Ni powder standard, is associated with reduced Ni particles in the zeolite. X-ray line broadening analysis (LBA) is useful in estimating average particle sizes in metal supported catalysts (24). Particles up to about 100 nm cause broadening of the diffraction lines (25). The extent of broadening is given by the Scherrer formula,

$$t = 0.9\lambda/(B\cos\theta_B) \quad [8]$$

where λ is the wavelength of X-rays used (1.54060 Å for CuKα radiation), B = broadening of diffraction lines

measured at half its maximum intensity (radians), θ_B is the angle of diffraction corresponding to the peak broadening and t = diameter of crystal particle. LBA is believed to be applicable in the range of 100 nm to about 1.5 nm (23). The standard for calibration of angles was quartz.

4. *Scanning electron microscopy (SEM).* SEM experiments were done with a AMRAY Model 1810 D microscope. Samples were mounted to a stainless steel holder with carbon-black paste. Location of reduced Ni on the surface of the zeolite was accomplished by using an AMRAY PV 9800 energy dispersive X-ray analyzer (EDX). EDX enables one to differentiate between Ni on the surface and the aluminosilicate support itself.

5. *Fourier transform infrared spectroscopy.* Fourier transform infrared (FTIR) spectroscopy experiments were performed on a Mattson Galaxy spectrometer with a home-built *in situ* IR cell. Each sample of Ni/NaX zeolite was doped with 20 wt% silicalite (Union Carbide), used as an internal calibration standard. Exactly 15 mg of doped sample was pressed into a pellet and placed in the IR cell. Each sample was dehydrated at 380°C for 8 h under a vacuum of 2×10^{-5} Torr. Dehydration temperature was reached by slowly increasing the temperature from room temperature to 380°C at a rate of 50°C/h.

Acidity was measured relative to the internal standard and by comparing the peak areas of Brønsted sites to Lewis sites. The analysis of chemisorbed pyridine on the zeolite at ambient temperature is described elsewhere (18, 26). The peak at 1541 cm^{-1}, corresponding to Brønsted acidity, was integrated and compared to the integrated peak area of the silicalite band at 2000 cm^{-1}. This was done in order to determine the relative number of Brønsted sites for the two loadings of Ni/NaX reduced under various conditions. The peak at 1541 cm^{-1} was also compared to the Lewis peak at 1460 cm^{-1} as well as the band at 2000 cm^{-1}. Silicalite, which does not have Brønsted or Lewis acidity, was chosen as a standard because of its intense band at 2000 cm^{-1} and because the framework Si–O vibrational bands of silicalite do not interfere in the pyridinium ion band for Brønsted or Lewis acidity. The aluminum content of silicalite was less than 300 ppm. Relative acidity measurements are used to account for changes in acidity upon reduction of the catalyst for different degrees of ion exchange. Absolute quantitative analysis of Brønsted and Lewis site populations cannot be done using FTIR analysis of adsorbed pyridine, because sample preparations will differ from one pellet to another.

6. *Electron paramagnetic resonance (EPR).* Electron paramagnetic resonance (EPR) measurements were carried out on a Varian E-3 ESR spectrometer at room temperature and 77 K near 9.1 GHz with 100 kHz magnetic field modulation.

III. RESULTS

A. Steady-State Kinetics

Experiments were run at various temperatures in order to obtain initial conversions of around 10–15% and steady-state conversions of 1–5%. Table 2 shows temperature ranges in which these conversions were achieved. Kinetic data obtained at these temperatures are those from which E_a values were derived. Rates of propylene formation, as well as gas phase propylene concentrations and conversions are reported in Table 3 for the high loading of Ni/NaX. Plots of rate as a function of acidity from 100 to 160°C for the high loading of Ni are shown in Fig. 1. Figure 2 is a plot of the log (Rate) as a function of acidity between 200 and 280°C for the low loading of Ni. Acidity is defined as the ratio of the absorbance area of the Brønsted (H^+) band to the silicalite band (S). These plots show that the rate of propylene formation increases with increasing reaction temperature. Increasing acidities result in increased reaction rates in c-C_3H_6 reactions. There was little difference in reaction rates between catalysts reduced at 350 and 450°C for 4 h. This result is observed in both the high loading and the low loading of Ni/NaX. Higher temperatures were required for steady state conversions of between 1–5% for the low loading of Ni/NaX.

A graph plotting propylene concentration as a function of time on stream for catalyst B at various temperatures is shown in Fig. 3. From this plot, near steady state conditions are apparent following 120 min of reaction. Propylene concentrations for catalysts with high loadings of Ni reduced under various conditions are plotted as a function of time on stream at 150°C in Fig. 4. The curves of Figs. 3 and 4 represent deactivation or poisoning of the

TABLE 2

Reaction Temperatures Required to Obtain between 1–5% Conversion at Steady-State and 10–15% Conversion Initially (Fresh Catalyst) in Isomerization Reactions over Various Catalysts.

Catalyst	Temperature (°C)
A	150–200
B	130–160
C	130–160
D	130–160
E	280–360
F	240–320
G	200–260
H	200–260

Note. Kinetic data obtained at these temperature ranges are used in calculating E_a.

TABLE 3

Isomerization Data for 0.5% c-C_3H_6 in He at 160°C over 10.7% Ni/NaX

Catalyst	Initial			Steady-State[a]		
	Conc.[b] $C_3H_6 \times 10^4$	Rate[c]	Conv.[d]	Conc.[b] $C_3H_6 \times 10^4$	Rate[c] $\times 10^8$	Conv.[d]
A	1.60	6.60	3.20	1.30	5.38	2.60
B	4.62	19.1	9.24	2.00	8.26	4.00
C	5.78	23.9	11.6	2.05	8.46	4.10
D	6.94	28.7	13.9	2.25	9.31	4.51

[a] After 125 min.
[b] mol%.
[c] mol/s · g.
[d] %.

catalyst in cyclopropane isomerization reactions over various Ni/NaX zeolites. These plots are typical for the mixed metal–acid catalysts studied in our experiments. Higher loadings of Ni and higher reaction temperatures result in greater rates of deactivation, as determined by the tangent to the deactivation curve. All variations in the reduction of highly loaded Ni/NaX catalysts have similar deactivation rates of approximately 4×10^{-1} μmol/g within the first hour of reaction. Figure 4 shows that deactivation of both catalysts B and C results in convergence at nearly the same steady state value of propylene concentration (2.3×10^{-2} mol%) after 120 min of reaction.

Nearly 100% regeneration of these isomerization catalysts can be obtained by heating at 380°C for 6 h in He. Reaction by-products sorbed on the surface of the catalyst in isomerization reactions have been observed to be a result of the reaction intermediate, which has been explained in terms of a π-allyl complex bound to the surface of Brønsted acid sites (27, 28).

Apparent activation energies have been determined for the isomerization reactions, and a typical plot is shown in Fig. 5. In this graph the slope of the line in the plot of ln (Rate) vs $1/T$ $(K)^{-1}$ is equal to E_a/R, where R is equal to 8.3145 J/mol · K. Figure 5 shows a linear relationship between ln (Rate) and T^{-1}, which suggests that this reaction is first order in propylene. Table 4 shows activation energies of the high and low loadings of Ni in NaX at various stages of reduction at initial time (t = 5 min) and at steady-state times (t = 125 min). Blanks in the table represent values in which correlation coefficients were below 0.95, and values may not be accurate within experimental error. These values are observed at initial times, when poisoning effects may vary significantly with temperature.

For the reaction of c-C_3H_6/H_2 studied on the catalysts with high loading of reduced Ni, propane, ethane, and methane were observed as products, while propylene was not. Figure 6 shows a typical concentration profile of products formed vs time on stream at 170°C for catalyst C. Propane hydrogeneration reactions have rates of 6.11×10^{-8} mol/s · g and 32% conversion, while hydrogenolysis reactions to methane and ethane have significantly slower rates of 2.22×10^{-8} mol · g or 10% conversion at 170°C over catalyst C. These values represent selectivities of around 10% for methane formation, 20%

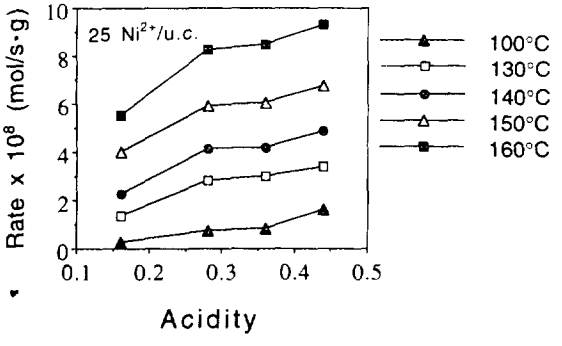

FIG. 1. Isomerization of c-C_3H_6. Plot of rate vs acidity between 100 and 160°C for the 10.7% Ni^{2+}/NaX catalysts A, B, C, and D. Acidity has been defined at the ratio of the integrated area of absorbance for Brønsted (H^+) to silicalite (S), the internal calibration peak.

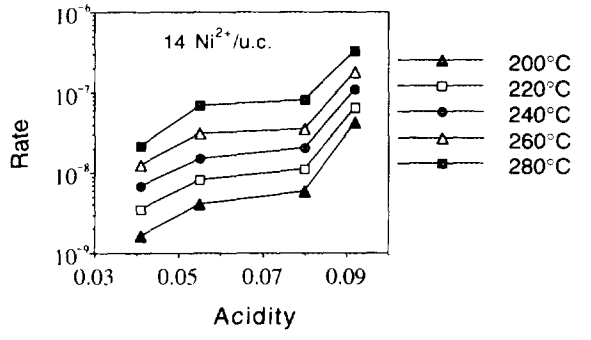

FIG. 2. Isomerization of c-C_3H_6. Semilog plot of rate vs acidity between 200 and 280°C for the 6.0% Ni^2/NaX catalysts E, F, G, and H.

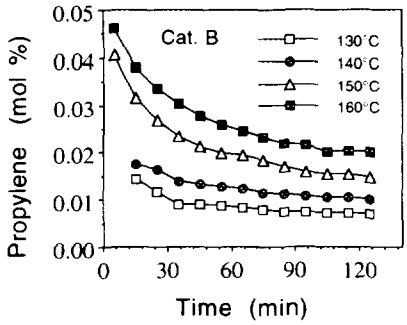

FIG. 3. Isomerization of c-C_3H_6. Gas composition of propylene vs time-on-stream for catalyst B at various temperatures.

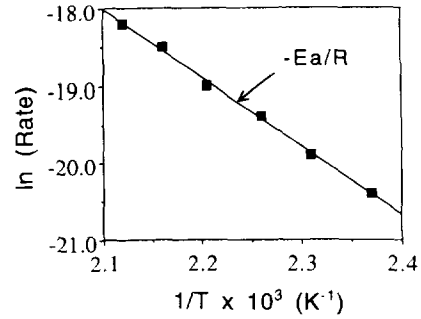

FIG. 5. Isomerization of c-C_3H_6 over catalyst A. Arrhenius plot of ln (Rate) vs $1/T \times 10^{-3}$ $(K)^{-1}$. Slope of line equals E_a/R.

for ethane, and 70% for propane. Similar selectivities were observed at other temperatures and on other catalysts tested. A 1 : 1 mole ratio of methane to ethane is observed, which is expected for hydrogenolysis reactions (29). Deactivation of these catalysts occurs more rapidly in hydrogenation reactions than hydrogenolysis reactions as depicted in Fig. 6. Catalyst reduction at 350°C (catalyst B) also produces some activity in hydrogenation and hydrogenolysis reactions; however, these rates are lower than samples reduced at higher temperatures by a factor of 10^{-2}.

B. Characterization

1. *AA.* Based on AA analyses, NaX exchanged with the 0.10 *M* solution of nickel nitrate was found to have a Ni weight percent of 10.7%, while the low loading (0.01 *M* exchange solution) had a Ni weight percent of 5.99%. Based on the composition of the unit cell for dehydrated NaX zeolite, $Na_{81}Al_{81}Si_{106}O_{374}$, values of 25 Ni^{2+} ions/unit cell for the high loading and 13.9 Ni^{2+} ions/unit cell for the low loading of Ni were calculated. This corresponds to a degree of exchange of 62% for the high loading of Ni and 34% for the low loading of Ni.

The Si-to-Al ratio of ion-exchanged materials was determined to be 1.31, consistent with the original composition of the starting material. AA analyses for Na^+ show that 2.96 and 6.18 wt.% Na^+ is present in the high and low loading of Ni^{2+}/NaX, respectively. Based on alkali and transition metal weight percents, the concentration of protons introduced following ion-exchange can be calculated. Based on an atomic balance for the unit cell of NaX (also determined experimentally), 8.0 and 3.2 H^+ have been added to the unit cell for the high and low loading of Ni^{2+}/NaX, respectively. The formulas of the high and low loading of Ni^{2+} in dehydrated NaX following cation exchange are, therefore, $H_8Na_{23}Ni_{25}Al_{81}Si_{106}O_{374}$ for the high loading of Ni in NaX and $H_{3.2}Na_{50}Ni_{13.9}Al_{81}Si_{106}O_{374}$ for the low loading.

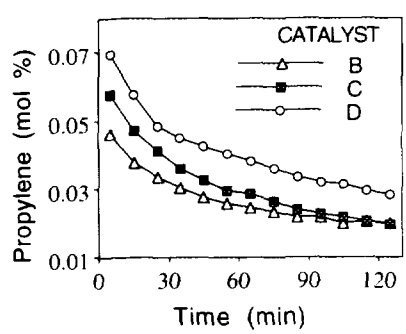

FIG. 4. Isomerization of c-C_3H_6. Gas composition of propylene vs time-on-stream for 10.7% Ni^{2+}/NaX at 150°C for reduced under various conditions.

2. *TPR data.* TPR spectra are shown in Fig. 7. The data show that 960 μmol/g of H_2 are necessary for complete reduction of the unreduced 10.7% Ni^{2+}/NaX catalyst A. Calibrations based on reduction of CuO confirm a Ni^{2+} weight percent of 10.9% which is in good agreement with atomic absorption studies. Sample B showed a reduction of 7.0 wt%, which is equivalent to 64% reduction of total Ni in the sample. Sample C had a reduction of 95% and Sample D was completely reduced after 19 h of reduction at 450°C.

TPR spectra of Fig. 7 were plotted out to 960 K (687°C)

TABLE 4

Apparent Activation Energies (E_a) for c-C_3H_6 Isomerization Reactions over Various Ni/NaX Catalysts

Catalyst	E_a (kJ/mol) Initial	Steady-State
A	[a]	71.6
B	70.2	52.3
C	55.1	51.5
D	[a]	35.5
E	95.4	70.2
F	85.4	67.7
G	84.9	62.7
H	56.5	60.9

[a] Poor fits to the Arrhenius relation.

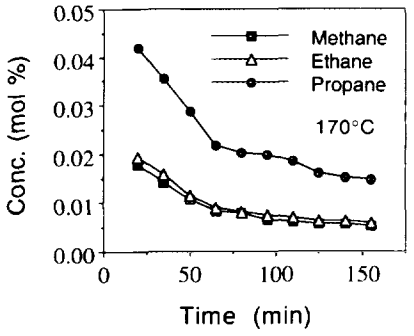

FIG. 6. Reaction of c-C_3H_6 in H_2. Hydrogenation to propane and hydrogenolysis to methane and ethane vs time on stream for catalyst C at 170°C.

in order to show that a negative signal is observed upon reduction at temperatures >860 K (587°C) for the unreduced sample and >770 K (497°C) for reduced samples. This negative peak corresponds to a generation of H_2 or other gas phase components.

3. *X-ray diffraction.* XRD patterns for catalysts A and D are shown in Fig. 8. Using the Scherrer formula for X-ray line broadening and a computer program to determine B, the extent of broadening at half peak maximum, particle sizes of 8.9 nm and 17.3 nm were obtained for samples C and D, respectively. Sample B showed no evidence of X-ray diffraction due to metallic Ni in the powder diffraction pattern. Ionic Ni^{2+} or Ni^{+} clusters in Ni/NaX were also undetectable when comparing the X-ray diffraction patterns to unexchanged NaX.

X-ray diffraction patterns for all catalysts of the low loading of Ni/NaX did not have peaks which correspond to Ni^0 centered at d = 2.015 Å and d = 1.747 Å. For this reason, only the high loading of Ni was effectively studied by X-ray LBA where line broadening was clearly evident.

4. *SEM data.* Unreduced Ni/NaX crystallites had particle sizes of 1 μm or greater, however, upon reduction

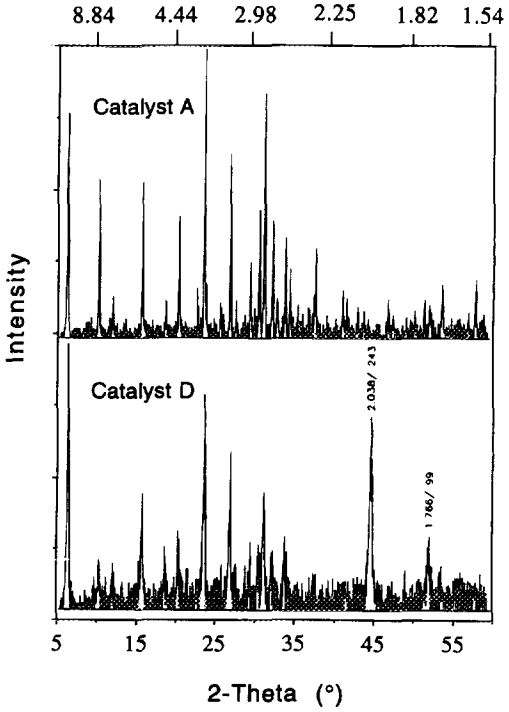

FIG. 8. X-ray diffraction pattern for catalyst A (Ni^{2+}/NaX) (top), and catalyst D, reduction at 450°C for 19 h (bottom). Step size 0.03°. Metallic Ni diffraction occurs at 44.8° and 52.5° 2θ and d-spacings of 2.029 and 1.747 Å.

at 450°C zeolite crystallite sizes decreased to 50–100 nm. Longer reduction times and higher reduction temperatures resulted in smaller zeolite crystallite particle sizes. EDX analysis on several fields of reduced Ni/NaX showed between 70–90% coverage of Ni on the surface of the zeolite in Sample D.

5. *FTIR data.* A typical infrared spectrum of adsorbed pyridine on catalyst D is shown in Fig. 9. Acidity analyses are made by integrating the standard internal calibration

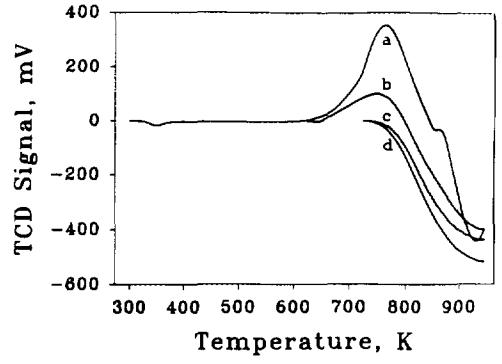

FIG. 7. Temperature programmed reduction from 298 to 970 K at a heating rate of 15°C/min for 10.7 wt% Ni/NaX. Sorption gas was 4% H_2/Ar, desorption purge was Ar (30 cm^3/min). Curve (a), unreduced Ni^{2+}/NaX; curve (b), reduced at 350°C for 4 h; curve (c), reduced at 450°C for 4 h; and curve (d), reduced at 450°C for 19 h.

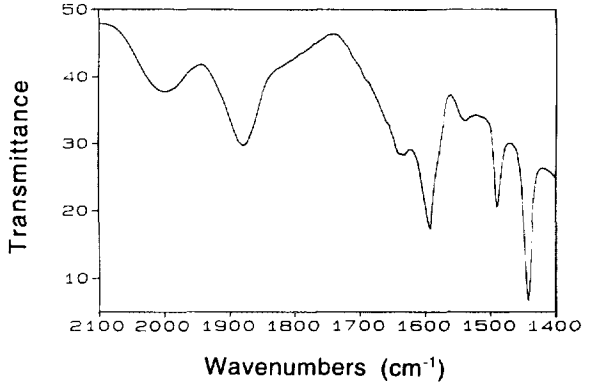

FIG. 9. Fourier transform infrared spectrum of pyridine chemisorbed on a Ni/NaX zeolite. Dehydration of zeolite at 380°C, followed by room-temperature sorption of pyridine, and then removal of physisorbed pyridine for 8 h at 150°C and 1 × 10^{-5} Torr.

TABLE 5

Acidity Measurements after Pyridine Adsorption on Various Ni/NaX Catalysts

Catalyst	H^+/S^a	H^+/Lewis[b]
A	0.16	5.672
B	0.28	7.920
C	0.36	8.133
D	0.44	8.837
E	0.041	5.892
F	0.055	5.878
G	0.080	7.379
H	0.092	7.388

[a] Ratio of Brønsted sites to the internal calibration peak of silicalite.
[b] Relative ratio of Brønsted to Lewis sites.

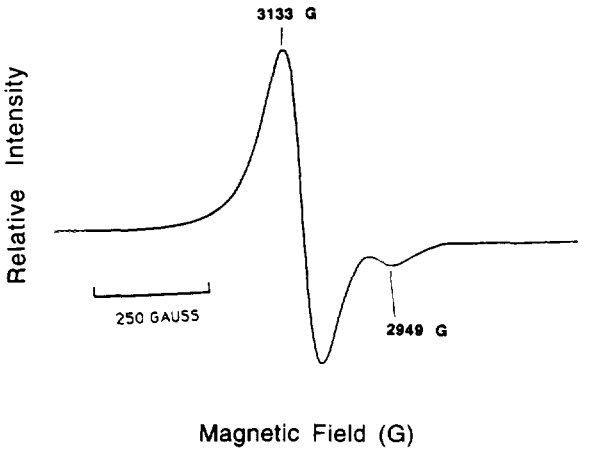

FIG. 11. Room temperature EPR spectrum of partially reduced 6.0% Ni/NaX zeolite (catalyst B). Frequency near 9.1 GHz.

peak of silicalite (S) at 2000 cm^{-1} and the peak corresponding to the pyridinium ion at 1541 cm^{-1}, which is related to Brønsted (H^+) acidity. A ratio of the two peak areas, in terms of transmittance, is used to compare the relative acidities from one catalyst reduction treatment to the other. The area of the Lewis peaks corresponding to physisorbed pyridine is also measured. These values are reported in Table 5 and the H^+/S (Brønsted/Silicalite) ratios are plotted vs catalyst treatment in Fig. 10.

6. *EPR.* The EPR spectrum of catalyst B is show in Fig. 11. This spectrum has an intense but broad peak at a magnetic field of 2949 G and a smaller peak at a magnetic field of 3133 gauss. The first peak has a g value of 2.191 and the smaller peak has a g value of 2.063. The peak centered at 2949 G has been assigned to Ni^0 in NaX. The peak centered at 3133 G has been assigned to Ni^+ in NaX. These g values are consistent with those reported in the literature for Ni/NaY (31–34). EPR spectra taken on samples heated to 450°C in H_2 do not show a peak corresponding to Ni^+.

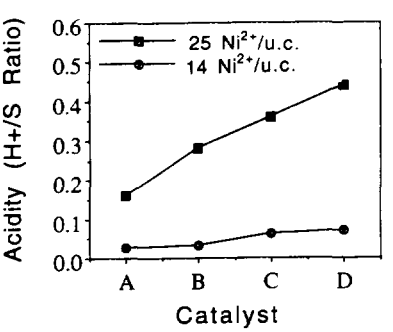

FIG. 10. Plot of acidity for 10.7 and 6.0% Ni/NaX as a function of various reduction treatments.

IV. DISCUSSION

A. Characterization: Ion-Exchange, Acidity, Reduction, Particle Size

Ion-exchange of Ni^{2+} in NaX in aqueous media occurs readily at room temperature. Degree of exchange nearly doubled as the concentrations of ion-exchange solutions increase from 0.01 M to 0.10 M. Similar degrees of ion-exchange were observed in previous work for exchange of Eu^{3+} ions in NaX zeolites (18).

Alkali and transition metal analyses reveal that protons have been introduced to both the high and low loading of nickel in NaX zeolites. Calculations based on the unit cell for NaX show that 8.0 H^+ ions and 3.2 H^+ ions per unit cell have been introduced in the high and low loadings of Ni^{2+}/NaX, respectively. The addition of protons into the zeolite following ion exchange and washing with water is likely to occur due to the acidic nature of nickel nitrate solutions. The 0.10 M and 0.01 M solutions of $Ni(NO_3)_2$ were found to have a pH of 5.095 and 6.087, respectively. Subsequent washings with water to remove nitrate counterions are likely to result in the addition of protons to the zeolites. The dissociation of water molecules under acidic conditions with formation of protons in zeolites occurs during exchange. FTIR analyses showing initial Brønsted acidity prior to reduction are also consistent with these results.

Reduction at 450°C on the high loading of Ni in NaX zeolites resulted in the formation of large Ni clusters at the surface of the zeolite crystallites as evidenced by SEM/EDX, and LBA in X-ray diffraction analyses. Agglomeration of Ni particles on the external surface of the crystallites at higher reduction temperatures (>400°C) is consistent with previous literature reports for Ni/NaY zeolites (35–38). The absence of X-ray line broadening in

the low loading suggests that agglomerated Ni particles are not present. This might be explained by a small amount of Ni^{2+} present in the supercages of NaX, where sintering of Ni particles occurs.

Total reduction of Ni was observed in the high loading of NaX zeolites at 450°C. Longer H_2 reduction treatment times resulted in formation of larger particles on the surface of the crystallites. The TPR data suggest that 100% of Ni in NaX can be reduced at higher temperatures. Temperatures below 450°C result in only partial reduction of the samples, with little or no sintering of particles detected.

The TPR data show that above 500°C reduced samples show a generation of H_2. This is consistent with degradation of the zeolite framework and/or oxidation of Ni^0 back to Ni^{2+}. XRD shows no additional peaks in the diffraction pattern that might correspond to Al_2O_3 or $NaAlO_2$ species, suggesting that dealumination is not a factor. An overall decrease in peak intensities is observed suggesting a decrease in crystallinity of this material. TPR data also suggest that more severe reduction treatments lower the overall stability of the zeolite.

From the TPR data, incomplete reduction is observed at lower temperatures (350°C) when the zeolite framework is still intact (as evidenced by XRD and SEM). Strong electrostatic interactions between Ni^{2+} cations and the negatively charged framework of the sodalite cages of NaX stabilize its cationic form, making reduction of Ni very difficult at low temperatures. Difficulty of reduction at low temperatures observed in this study is consistent with earlier reports which reveal similar difficulties in the reduction of Ni in faujasite zeolites (39, 40). Thomas *et al.* reported in TPR studies on NaY that only 30% of the total Ni^{2+} content was reduced at 500°C while 80% reduction was observed at 900°C (39). Dooryhee *et al.* reported that only 20% of Ni^{2+} was reduced at 450°C for 32 h in a 9% Ni^{2+} exchanged NaY zeolite (40).

NaY zeolites are more stable than NaX zeolites, used in these experiments. Degradation of the zeolite framework is observed above 400°C. Reduction at 450°C begins to destroy the framework structure which may enhance the reduction procedure. This is not the case in the more stable NaY zeolite. Deformation of the zeolite framework eliminates strong interactions between Ni^{2+} and the negatively charged framework and frees Ni^{2+} ions from the protective sodalite cages. Low temperature reductions have been attributed to Ni^{2+} at site IIa, near the supercage, and high temperature reductions to Ni^{2+} in site I, I′, and II in the hexagonal prisms and sodalite cages. A decrease in intensity of X-ray diffraction peaks in the reduced samples and SEM analyses, which show a significant reduction in crystallite size, suggest that deformation of the zeolite structure occurs upon reduction at higher temperatures (450°C).

Location of Ni^{2+} ions, reduction conditions, and catalyst calcination and dehydration treatments, are important factors that influence Ni^{2+} reduction in the zeolite. Ni^{2+} has been reported to be octahedrally coordinated to framework oxygen in the hexagonal prism at the entrance to the sodalite cage and trigonal or tetrahedrally coordinated with the 6-single rings of the sodalite cage or in the center of the sodalite cage itself (41–43). Saturated coordination of Ni^{2+} in the hexagonal prism makes reduction of these cations more difficult than those located in the sodalite and supercages which are coordinatively unsaturated (44). The density of negative charge is highest in the small cages, therefore site occupancy is energetically favored with the divalent Ni^{2+} cations in the sodalite cages and the monovalent Na^+ ions in the supercage. High temperatures are required for reduction of Ni^{2+} ions located in sites I and I′ (44), although some authors report that Ni^{2+} ions in site I are easily reduced (45, 46). Reduction of Ni^{2+} in faujasite zeolites is usually incomplete (47, 48). This is consistent with the low temperature reductions observed in our studies.

Higher degrees of ion-exchange of Ni^{2+} observed in the 10.7% Ni/NaX samples, result in higher populations of Ni^{2+} ions in the supercage, which may be readily reduced (and sintered). Literature reports suggest that the degree of reduction of Ni^{2+} cations supported on zeolites is dependent on the level of nickel exchange and the Brønsted acidity associated with the zeolite (49). This is consistent with catalytic acitivity in hydrogenation reactions which show higher conversions at lower temperatures with the higher loadings of Ni/NaX, suggesting that there are more available Ni^0 sites and therefore a higher degree of reduction. Also, the faujasite zeolites show a decrease in reduced nickel with increasing acidity (50, 51). This is inconsistent with initial acidity measurements in this study which show that the higher loading of Ni has higher acidity prior to reduction than the low loading, yet the extent of reduction is more complete in the high loading. In this comparison it must be concluded that differences in the location of Ni^{2+} cations as a result of the degree of ion exchange in the samples are more significant than differences in acidity in NaX zeolite. This is consistent with earlier reports which suggest that differences in Ni^{2+} loadings have resulted in different reduction behavior (52). Based on the relative Brønsted-to-silicalite ratio determined by chemisorbed pyridine in our analyses, initial acidities of Ni^{2+} exchanged zeolites are very low.

EPR and FTIR studies of chemisorbed CO on Ni^+ ions located in sodalite cages reveal that the complexed $Ni(CO)^+$ species migrate to the supercage at room temperature (53). The driving force for ion mobility appears to be due to coulombic interactions and interactions between the cation and the negatively charged framework. Charge density in the zeolite also controls cation location and

mobility. Mobility of Ni^{2+} ions can be reduced by introducing large trivalent ions into the zeolite thereby populating the sodalite cages with these ions, leaving the supercages to be occupied by Ni^{2+} and remaining Na^+ ions. This favors trigonally coordinated Ni^{2+} in the supercages which can be readily reduced (54).

Upon reduction with H_2 a marked increase in Brønsted acidity is observed. This is consistent with previous mechanistic ideas as shown in [9]:

$$Ni^{2+} + H_2(g) \rightarrow Ni^0 + 2H^+_{zeolite} \qquad [9]$$

In earlier work with lanthanide ion-exchange (Eu^{3+} in particular) the generation of Brønsted acidity was explained by the dissociation of water molecules and the formation of lanthanide oxide complexes in the sodalite cages of the zeolite. At present, we have no experimental data to either prove or disprove this occurrence in the nickel system. As previously discussed, initial Brønsted acidities of Ni^{2+}/NaX zeolites prior to reduction are likely to result from $Ni(NO_3)_2$ solutions themselves which are acidic, see Eq. [10]. This observation is consistent with both FTIR chemisorption experiments and elemental analyses which show that protons have been introduced into Ni^{2+}/NaX zeolites following ion exchange and subsequent washings with DDW. Increased initial Lewis acidities may result from Ni^{2+} ions themselves which may sorb pyridine in FTIR chemisorption experiments. It has been suggested that vacant *d*-orbitals of Ni^{2+} may account for the adsorption of pyridine (55).

$$2Ni^{2+} + H_2O \rightarrow 2Ni^+ + 2H^+_{zeolite} + \tfrac{1}{2}O_2 \qquad [10]$$

Reduction generates hydroxyl groups in the smaller cages and also causes migration of the supercage protons to inaccessible sites (48). This is consistent with the observation that an increase in Brønsted acidity is observed upon reduction of Ni. Reduction of Ni in the supercage and Ni^{2+} ion migration out of the sodalite cage at elevated temperatures would produce Brønsted acidity primarily in the sodalite cage in order to maintain charge neutrality. An increased uptake in pyridine may be explained in terms of a competition between newly formed Brønsted sites as a result of reduction and site occupancy due to Ni^{2+} ion migration at higher reduction temperatures. We also expect that a partial collapse of the zeolite structure under the most severe reduction conditions studied might make H^+ sites more accessible to pyridine and c-C_3H_6 in chemisorption measurements and reaction studies. This may be an explanation for the fact that increased pyridine uptakes in samples C and D are observed even though they have nearly equal amounts of reduced Ni. Coughlan and Keane reported that in low loaded zeolites (<6 Ni^{2+}/U.C.) protons are located only in the supercages (56). This is consistent with acidity measurements for the low loading of Ni^{2+} in NaX in our studies prior to reduction treatments. This has also been observed in previous work (55).

Reduction treatments not only affect catalytic activity, reaction rates and activation energies, but also the oxidation states of Ni and the chemistry of the catalyst. It has been reported in zeolites containing low concentrations of Ni^{2+} that Ni^0 particles migrate into the sodalite cages to react with Ni^{2+} ions to form monovalent Ni^+ species (53). This disproportionation reaction occurs only at low reduction temperatures and if Ni atoms do not agglomerate (which could prevent diffusion of H_2 into the sodalite cages). In order for monovalent Ni^+ species to form, reduction temperatures must be kept below 400°C and Ni^{2+} concentrations must be low. This reduction reaction has been observed in EPR measurements on the low loading of Ni/NaX (6.0% Ni) which show the presence of Ni^+ upon reduction at 350°C. The *g* value of 2.063 observed for the Ni^+ signal is consistent with previous reports of Ni^+ in NaY (31). The presence of Ni^+ is understandable due to incomplete reduction of Ni. Upon further reduction at 450°C, however, EPR signals corresponding to Ni^+ ions are no longer present as shown in Eq. [11]:

$$Ni^{2+} \xrightarrow{350°C} Ni^+ \xrightarrow{450°C} Ni^0 \qquad [11]$$

B. Steady-State Kinetics

c-C_3H_6 isomerization reactions occur on Brønsted sites in Ni/NaX zeolites. These reactions were found to take place readily between 100 and 160°C for the high loading of Ni/NaX, but require much higher temperatures (250–340°C) for the same conversions in the low loading. Presumably, this is a result of lower turnover frequencies due to less available Brønsted sites to catalyze this reaction in the low loading. This is consistent with acidity measurements previously described for these systems. There was little difference observed in activity between catalysts reduced at 350°C and 450°C for 4 h both in the high and low loadings of Ni. This may be a result of increased site occupancy in the sodalite cages of NaX under reduction at higher temperatures, where c-C_3H_6 cannot diffuse. This process occurs when Ni^{2+} ions migrate from the sodalite cage into the supercage upon reduction. To maintain charge neutrality H^+ ions reside in the sodalite cages.

Apparent activation energies ranged from 71.6 kJ/mol to 35.5 kJ/mol for isomerization reactions at steady-state. Higher activation energies were observed for nonreduced catalysts. Increased degrees of reduction resulted in a decrease in activation energies by as much as 16.8 kJ/mol. In comparing the two loadings of Ni at steady-state, the higher loading had activation energies between 15.4 and 25.4 kJ/mol lower than the low loading in reduced

catalysts. Similar activation energies were observed for both the high and low loading of unreduced Ni/NaX. This suggests that increased degrees of reduction result in lower activation energies. In terms of acidity (not reduction), these same trends were observed in earlier work for studies of isomerization reactions with acid catalysts (18).

A relationship among the contribution of metal sites, cationic sites, and Brønsted sites in c-C_3H_6 isomerization reactions is difficult to determine. The proposed mechanism of c-C_3H_6 ring opening through a carbenium ion intermediate suggests that Brønsted acidity is necessary for isomerization. Earlier work with Na vapor poisoning on the Brønsted sites in Eu^{3+}-exchanged NaX showed that Lewis acidity did not contribute to ring opening at low temperatures (18). Reactions on metal sites provide no mechanism of ring opening and isomerization was not observed over high purity Ni powder (1 μm particles) up to 360°C. Increased reaction rates between nonreduced Ni^{2+}/NaX and reduced Ni/NaX are likely to be due to an increase in Brønsted acidity, a result of the reduction of Ni. c-C_3H_6/H_2 TPD studies show no evidence of propylene formation up to 240°C (55). This suggests that Ni^{2+} does not catalyze ring opening at low temperatures.

At higher temperatures (300°C) however, it was observed that catalytic activity increased almost linearly with time on stream for the partially reduced samples (catalysts B and F). These results suggest that Ni^+ or Ni^{2+} ions migrate from the hexagonal prisms located at the entrance of the sodalite cage into the supercage, where they are accessible to reactant molecules, at higher temperatures. Migration of Ni^+ or Ni^{2+} ions into the supercage at elevated temperatures has been reported in *in situ* X-ray powder diffraction studies (40). Therefore, we propose that Ni^+ and possibly Ni^{2+} ions are catalytically active in isomerization reactions at high temperatures (>280°C).

Sodium vapor reduction experiments on the high loading of unreduced Ni^{2+}/NaX were carried out in order to determine whether Ni^+ or Ni^{2+} cation sites were indeed active in c-C_3H_6 isomerization reactions. Na vapor deposition methods have been described in earlier work (57). This method of reduction allows incomplete reduction of nickel to primarily the monovalent Ni^+ ion with some complete reduction to Ni^0 (34) without generating acid sites as in H_2 reduction. Previous work on the deposition of sodium vapor has proven to eliminate Brønsted acidity in zeolites (18). The reduction of Brønsted sites (hydroxyl groups) is shown in Eq. [12].

$$Na^0 + H^+_{zeolite} \rightarrow Na^+ + \tfrac{1}{2} H_2(g) \qquad [12]$$

Pyridine chemisorption experiments on Na vapor treated Ni^{2+}/NaX zeolites also show that Brønsted acidity is eliminated. This is consistent with earlier work on lanthanide-exchanged NaX zeolites (18). Catalytic results for Na vapor treated NiX show that conversions of 5–10% can be obtained at higher temperatures of between 280–320°C. This suggests that Ni^+ ions (and not Ni^{2+} ions) are catalytically active in ring opening reactions up to 320°C.

When Na vapor was applied to NaX zeolite (not cation-exchanged), sodium ionic clusters having the formula Na_4^{3+} were formed in the sodalite cages of the zeolite (57). FTIR acidity measurements on these materials also show that Brønsted acidity has been completely eliminated on these materials. The effects of sodium vapor treatments on NaX zeolite are very different from those on lanthanide or transition metal cation exchanged zeolites (18, 57).

It has been reported that Ni in its cationic form is a potential catalyst for hydrocarbon transformations (58). Monovalent Ni^+ cations have been indicated to be catalytically active in ethylene dimerization reactions (59). CO adsorption to Ni^+ ions have also been observed (53), confirming the acidic nature of Ni^+ which is necessary for ring opening. Cationic nickel interacts with framework oxygens but can also possess free coordination sites for interaction with reactants (40). Further, transition metal-exchanged zeolites, both in their unreduced and reduced form, are known to be powerful catalysts for a wide range of organic reactions, including oxidation, hydrogenation, and isomerization. The catalytic properties of these cations are therefore controlled by their location in the zeolite cavities and accessibility to c-C_3H_6 and upon their coordination to the framework.

Higher reaction temperatures were required for the low loading of Ni to achieve conversions at the level of the high loading of Ni. Further, upon extended reduction times at higher temperatures, large Ni agglomerates are not apparent in the low loading of Ni. This suggests that a decrease in the degree of ion-exchange may account for a decreased population of Ni^{2+} ions in the supercage where reduction and particle agglomeration are thought to occur. With less Ni^{2+} ions available for reduction, the population of sites in which reduction of Ni in the catalyst could occur, i.e., sites II and II′, is expected to be very much lower than those of the high loading. Thus, particle migration and agglomeration should not be a major factor in the low loading as it may be in the high loading where much higher degrees of reduction were observed. This is consistent with earlier reports that agglomeration occurs primarily for high loading of Ni^{2+} in zeolites (38).

Hydrogenation and hydrogenolysis reactions were observed over both loadings of Ni/NaX. Hydrogenation to propane occurred at approximately three times the rate of hydrogenolysis to methane and ethane. These reactions were observed on 10.7% Ni in NaX between 130 and 170°C under similar conditions for isomerization reactions. Poisoning of the catalyst was at least 10 times more rapid in hydrogenation and hydrogenolysis reactions, de-

pending on conditions, than in isomerization reactions. Hydrogenation and hydrogenolysis were observed over freshly reduced Ni powder only at higher temperatures (>260°C). Yields over this catalyst were reduced to 3% CH_4, 1% C_2H_6, and 2.5% C_3H_8 at 260°C. These yields differ significantly from that of Ni dispersed on NaX zeolites. Further, 1 : 1 mole ratios of methane to ethane, typical in hydrogenolysis reactions over acid catalysts (29), were not observed over high purity Ni powder, and methane was the favored product.

As mentioned earlier, propylene was not observed when c-C_3H_6 in H_2 was used as a feed mixture. The absence of propylene in the temperature range studied is expected due to the low concentration of reactant and high concentration of H_2 in the gas feed.

Regeneration of these catalysts was not possible using He at 380°C. This is unlike isomerization reactions over Brønsted sites whereby complete restoration of the catalyst could be achieved under flowing He at 380°C. Regeneration studies showed that under H_2, desorbed products were primarily methane; however, this process was not useful in our experiments because regeneration in H_2 would presumably increase Ni reduction. In our studies, therefore, freshly reduced catalysts were used in each analysis. Similarly, O_2 used as a regeneration gas would potentially destroy catalytic activity of the catalyst upon formation of NiO species. Reduction of the oxide may not result in exactly the same degree of reduction from one catalyst to another, making comparisons under different reaction conditions difficult. However, upon regeneration in O_2 at 380°C, CO_2 was the primary desorbed product.

V. CONCLUSIONS

Ion-exchange of Ni^{2+} cations for Na^+ in NaX zeolites can be easily achieved at room temperature. Interactions between Ni^{2+} ions and the zeolite framework inhibit the reduction process at low temperature. An excess of Ni^{2+} in the 0.10 *M* exchanged zeolite presumably creates a high population of Ni^{2+} ions in the supercages which enables the formation of larger Ni particles on the surface of these materials upon reduction. Reduction of Ni^{2+} in highly exchanged zeolites results in particle migration and agglomeration on the surface of the crystallites at higher reduction temperatures as shown by X-ray line broadening.

Deformation of the zeolite framework is observed in the XRD and in SEM upon reduction at higher temperatures. The low Si/Al ratio in NaX zeolites reduces the stability of these materials at high temperatures (>400°C). The extent of reduction increases with increasing reduction temperature. This increase in reduction may be a result of the deformation of the zeolite framework under reduction conditions.

Ni^+ ions are observed by EPR measurements upon reduction at 350°C. Higher reaction temperatures result in an increase in activity in isomerization. This is explained in terms of the mobility of Ni^+ and Ni^{2+} cations from the sodalite cage to the supercage, where catalytic activity occurs. This suggests that cationic nickel is catalytically active for isomerization at temperatures greater than 300°C. Na vapor studies and TPD results suggest that Ni^+ ions (and not Ni^{2+} ions) are catalytically active up to 320°C.

Increased Brønsted acidity results in lower activation energies, higher conversions, and faster reaction rates. Reduction of Ni^{2+} shows a marked increase in Brønsted acidity, as shown by FTIR analysis after pyridine adsorption.

Hydrogenation reactions to propane are observed over reduced Ni/NaX zeolites. Reaction rates and deactivation in hydrogenation reactions are up to 10 times greater than hydrogenolysis reactions to methane and ethane, depending on temperature.

c-C_3H_6 isomerization reactions were readily observed at low temperatures over cation-exchanged Ni^{2+}/NaX zeolites. Isomerization reactions were observed for the unreduced form of Ni/NaX. FTIR analyses of adsorbed pyridine show that Brønsted acidity exists prior to reduction. This is consistent with elemental analyses of Na^+ and Ni^{2+} which reveal that protons have been introduced into the zeolite following ion exchange with nickel nitrate solutions.

The isomerization activity on the catalyst was regenerated completely with He at 380°C. Hydrogenation and hydrogenolysis activities on the catalysts could not be regenerated in He, but H_2 and O_2 were found to be effective in restoring the catalyst to original conversion levels.

ACKNOWLEDGMENTS

The authors thank Wen-Qing Xu for TPR data and Roberto DeGuzman for EPR data. We also acknowledge the support of the Department of Energy, Office of Basic Energy Sciences, Division of Chemical Sciences for this research.

REFERENCES

1. Rabo, J. A., Schomaker, V., and Pickert, P. E., *Proc. Int. Congr. Catal. 3rd*, St. 2, No. 6 (1964).
2. Van Sickel, D. E., and Prest, M. L., *J. Catal.* **19,** 209 (1970).
3. Mochida, I., Hayata, S., Keto, A., and Seiyama, T., *J. Catal.* **15,** 314 (1968); **23,** 31 (1971).
4. Yashima, T., Ushida, Y., Ebisawa, M., and Hara, N., *J. Catal.* **36,** 320 (1975).
5. Roberts, R. M., *J. Phys. Chem.* **63,** 1400 (1959).
6. Fejes, P. Hannus, I., Kiricsi, I., Varga, K., Symposium on Zeolites, Szeged, Hungary, 1978. *Acta Phys. Chem.* **24,** 119 (1978).
7. Hall, W. K., Lutinshi, F. E., and Gerberich, H. R., *J. Catal.* **3,** 512 (1964).

8. Flockhart, B. D., McLoughlin, L., and Pink, R. C., *J. Chem. Soc. Chem. Commun.* 818 (1970).
9. Bond, G. C., and Sheridan, J., *Trans. Faraday Soc.* **48,** 713 (1952).
10. Bond, G. C., and Newham, J., *Trans. Faraday Soc.* **56,** 1501 (1960).
11. Benson, J. E., Kwan, T., *J. Phys. Chem.* **60,** 1601 (1956).
12. Taylor, W. F., Yates, J. C., and Sinfelt, J. H., *J. Catal.* **4,** 374 (1965).
13. Knor, Z., Ponec, V., Herman, Z., Dolejsek, Z., and Cerny, S., *J. Catal.* **2,** 299 (1963).
14. Addy, J., and Bond, G. C., *Trans. Faraday Soc.* **53,** 368, 377, 383 (1957).
15. Bond, G. C., and Turkevich, J., *Trans. Faraday Soc.* **50,** 1335 (1954).
16. Bond, G. C., "Catalysis by Metals," p. 271. Academic Press, New York, 1962.
17. Taylor, W. F., Yates, D. J. C., and Sinfelt, J. H., *J. Phys. Chem.* **68,** 2962 (1964).
18. Simon, M. W., Efstathiou, A. M., Bennett, C. O., and Suib, S. L., *J. Catal.* **138,** 1 (1992).
19. Roginski, S. Z., and Rathmann, J., *J. Am. Chem. Soc.* **55,** 2800 (1933).
20. Stevens, S. J., *J. Phys. Chem.* **62,** 714 (1955).
21. Coenen, J. W. E., Schats, W. M. T. M., van Meerten, R. Z. C., *Bull. Soc. Chim. Belg.* **88,** 435 (1979).
22. Bertucco, A., and Bennett, C. O., *Appl. Catal.* **35,** 329 (1987).
23. Che, M., and Bennett, C. O., *Adv. Catal.* **36,** 55 (1989).
24. Cullity, B. D., "Elements of X-ray Diffraction," p. 284, Addison–Wesley, Reading, MA, 1978.
25. Gallezot, P., *Catal. Sci. Technol.* **5,** 221 (1984).
26. Simon, M. W., Nam, S. S., Xu, W.-Q., Suib, S. L., Edwards, J. C., and O'Young, C.-L., *J. Phys. Chem.* **96,** 6381 (1992).
27. Kirisci, I., and Förster, H., *J. Chem. Soc. Faraday Trans. 1* **84**(2), 491 (1988).
28. Liengme, B. V., and Hall, W. K., *Trans. Faraday Soc.* **62,** 3229 (1968).
29. Satterfield, C. N., "Heterogeneous Catalysis in Industrial Practice," 2nd Ed., p. 176, McGraw-Hill, New York, 1991.
30. (a) Efstathiou, A. M., Borgstedt, E. v. R., Suib, S. L., and Bennett, C. O., *J. Catal.* **135,** 135 (1992); (b) Efstathiou, A. M., Suib, S. L., and Bennett, C. O., *J. Catal.* **123,** 456 (1990).
31. Kermarec, M., Olivier, D., Richard, M., Che, M., and Bozon-Verduraz, F., *J. Phys. Chem.* **86,** 2818 (1982).
32. Schoonheydt, R. A., and Roodhooft, D., *J. Phys. Chem.* **90,** 6319 (1986).
33. Ghosh, A. K., and Kevan, L., *J. Phys. Chem.* **94,** 3117 (1990).
34. Rabo, J. A., Angel, C. L., Kasai, P. H., and Schomaker, V., *Discuss. Faraday Soc.* **43,** 328 (1966).
35. Jacobs, P. A., Nijs, H., Verdonck, J., Derouane, E. G., Gilson, J.-P., and Simoens, A. J., *J. Chem. Soc. Faraday Trans. 1* **75,** 1196 (1979).
36. Briend-Faure, M., Jeanjean, J., Kermarec, M., and Delafosse, D., *J. Chem. Soc. Faraday Trans. 1* **74,** 1538 (1978).
37. Feeley, J. S., and Sachtler, W. M. H., *Catal. Lett.* **9,** 377 (1991).
38. Guilleux, M. F., Delafosse, D., Martin, G. A., and Delmon, J. A., *J. Chem. Soc. Faraday Trans. 1* **75,** 165 (1979).
39. Thomas, J. M., Williams, C., and Rayment, T., *J. Chem. Soc. Faraday Trans.* **84**(9), 2915 (1988).
40. Dooryhee, E., Catlow, C. R. A., Couves, J. W., Maddox, P. J., Thomas, J. M., Greaves, G. N., Steel, A. T., and Townsend, R. P., *J. Phys. Chem.* **95,** 4514 (1991).
41. Woolery, G., Kuehl, G., Chester, A., Bein, T., Stucky, G., and Sayers, D. E., *J. Phys. C* **8,** 281 (1986).
42. Schoonheydt, R. A., Roodhooft, D., and Leeman, H., *Zeolites* **7,** 412 (1987).
43. George, A. R., Catlow, C. R. A., and Thomas, J. M., *Catal. Lett.* **8,** 193 (1991).
44. Schoonheydt, R. A., and Roodhooft, D., *J. Phys. Chem.* **90,** 6319 (1986).
45. Egerton, T. A., and Vickerman, J. C., *J. Chem. Soc. Faraday Trans. 1* **69,** 39 (1973).
46. Schrubbers, H., Schultz-Ekloff, G., and Wildeboer, H., *Stud. Surf. Sci. Catal.* **12,** 261 (1982).
47. Briend-Faure, M., Guilleux, M. F., Jeanjean, J., Delafosse, D., Djega, Mariadassou, G., and Bureau Tardy, M., *Acta. Phys. Chem.* **24,** 99 (1978).
48. Briese-Gulban, S., Kompa, H., Schrubbers, H., and Schulz-Ekloff, G., *React. Kinet. Catal. Lett.* **20,** 7 (1982).
49. Coughlan, B., and Keane, M. A., *J. Catal.* **136,** 170 (1992).
50. Richardson, J. T., *J. Catal.* **21,** 122 (1971).
51. Suzuki, M., Tsutsumi, K., and Takahashi, H., *Zeolites* **2,** 51 (1982).
52. Coughlan, B., and Keane, M. A., *J. Catal.* **123,** 364 (1990).
53. Kermarec, M., Olivier, D., Richard, M., Che, M., and Bozon-Verduraz, F., *J. Phys. Chem.* **86,** 2818 (1982).
54. Schoonheydt, R. A., Vaesen, I., and Leeman, H., *J. Phys. Chem.* **93,** 1515 (1989).
55. Efstathiou, A. M., Suib, S. L., Bennett, C. O., *J. Catal.* **135,** 236 (1992).
56. Coughlan, B., and Keane, M., *J. Colloid and Interface Sci.* **137**(2), 483 (1990).
57. Simon, M. W., Edwards, J. E., and Suib, S. L., submitted.
58. Maxwell, I. E., *Adv. Catal.* **31,** 1 (1982).
59. Bonnevoit, L., Olivier, D., and Che, M., *J. Mol. Catal.* **21,** 415 (1983).